SMAR 2019

Remote microtremor monitoring of railway bridge pier for scour detection

Shinji KITAGAWA [1], Masaki SHINODA [1], Hironobu YAO [1], Chul-Woo KIM [2],
Yoshinao GOI [2], Kazuhiro YOSHITOME [2], Yoshisada HAMADA [3]

[1] Fuji Electric Co. LTD., Tokyo, Japan

[2] Kyoto University, Kyoto, Japan

[3] West Japan Railway Company, Osaka, Japan

Contact e-mail: kim.chulwoo.5u@kyoto-u.ac.jp

ABSTRACT: The impact test on the railway bridge pier to identify changes in frequencies has been adopted as a promising scour detection method in Japan. This study investigates feasibility of vibration-based scour monitoring as an alternative method for the impact test, as the impact test is a laborious and time-consuming method and is inapplicable for the real time monitoring to make a proper decision on the train operation control during heavy rains. A railway bridge with high potential of scour has been being monitored utilizing a remote sensing unit. The monitored modal properties demonstrated extremely low possibility of scour occurrence.

1 INTRODUCTION

Scouring is the erosion of the riverbed caused by fluctuation in the flow of river, turbulence, etc. The number of bridges with scoured piers is increasing due to the deterioration, heavy rain, and the reduction of sediment supply volume (Keyaki and Suzuki 2013). If scouring occurs around the foundation ground, the substructure may settle, incline, or fall. For safety, the trains should be prohibited to pass on the bridges with the scoured substructures. Fatal accidents possibly occur if train forcedly passes over the scoured bridges. In Japan, an impact test on the railway bridge pier has been adopted as a promising scour detection method to identify changes in frequencies. However, the impact test is a laborious and time-consuming method, and is inapplicable for the real time monitoring during heavy rains to make a proper decision on the train operation. Therefore, a remote monitoring system and a decision rule to detect scouring are desired.

This study aims to propose a way to monitor scour of piers of railway bridges efficiently and quantitatively without approaching the target bridge especially during flood. A bridge under operation is monitored as a case study. To estimate the natural frequency of the target bridge, accelerometers are installed on top of the bridge pier and the connected girders for the impact test, and two sensors on the pier top were left for scour monitoring by means of the long-term ambient vibration monitoring. In modal identification of the bridge, this study utilizes time domain method called stochastic subspace identification (SSI) (Heylen et al. 1997, van Overschee and De Moor1996, Goi and Kim 2016) that is effective for bridges under impact loadings. Bayesian operational modal analysis (BAYOMA) (Au 2011, Au et al. 2013, Goi et al. 2016) is also adopted for the modal identification from ambient vibrations.

2 IDENTIFICATION OF VIBRATION CHARACTERISTICS

2.1 Mode Identification by Stochastic Subspace Identification

The dynamical system representing the pier vibration is modeled as the following state space model.

$$\mathbf{x}(k+1) = \mathbf{A}\mathbf{x}(k) + \mathbf{w}(k) \tag{1}$$

$$\mathbf{y}(k) = \mathbf{C}\mathbf{x}(k) + \mathbf{v}(k) \tag{2}$$

Therein, $\mathbf{x}(k)$ and $\mathbf{y}(k)$ denote the state of structure and measurement at each time step k, respectively. Also, $\mathbf{w}(k)$ and $\mathbf{v}(k)$ respectively denote the process noise and measurement noise vectors which are assumed to be stationary white noise. System matrix $\mathbf{A}$ comprising modal information is estimated using least-squares method for the minimal prediction error of the state $\mathbf{x}(k)$ given by the forward Kalman filter. The poles of the dynamical system provide modal properties of the dynamical system.

The algorithm for the SSI is described briefly as follows. First, we obtain the projection matrix $\boldsymbol{O}_i$, as estimated from Eq. (3).

$$\boldsymbol{O}_i = \mathbf{Y}_\mathrm{f}\mathbf{Y}_\mathrm{p}^\mathrm{T}\left(\mathbf{Y}_\mathrm{p}\mathbf{Y}_\mathrm{p}^\mathrm{T}\right)^\dagger\mathbf{Y}_\mathrm{p} \tag{3}$$

Therein $(\cdot)^\dagger$ denotes the Moore-Penrose pseudo-inverse matrix. $\mathbf{Y}_\mathrm{f}$ and $\mathbf{Y}_\mathrm{p}$ represent the block Hankel matrices of the future and past outputs as shown in Eq. (4) and Eq. (5).

$$\mathbf{Y}_\mathrm{p} = \begin{bmatrix} \mathbf{y}(0) & \mathbf{y}(1) & \dots & \mathbf{y}(j-1) \\ \dots & \dots & \dots & \dots \\ \mathbf{y}(i-2) & \mathbf{y}(i-1) & \dots & \mathbf{y}(i+j-3) \\ \mathbf{y}(i-1) & \mathbf{y}(i) & \dots & \mathbf{y}(i+j-2) \end{bmatrix} \tag{4}$$

$$\mathbf{Y}_\mathrm{f} = \begin{bmatrix} \mathbf{y}(i) & \mathbf{y}(i+1) & \dots & \mathbf{y}(i+j-1) \\ \dots & \dots & \dots & \dots \\ \mathbf{y}(2i-2) & \mathbf{y}(2i-1) & \dots & \mathbf{y}(2i+j-3) \\ \mathbf{y}(2i-1) & \mathbf{y}(2i) & \dots & \mathbf{y}(2i+j-2) \end{bmatrix} \tag{5}$$

The singular value decomposition (SVD) is then applied to factorize $\boldsymbol{O}_i$ as shown below.

$$\boldsymbol{O}_i = \mathbf{U}\mathbf{S}\mathbf{V}^\mathbf{T} \simeq (\mathbf{U}_1\mathbf{U}_2)\begin{pmatrix} \mathbf{S}_1 & \mathbf{0} \\ \mathbf{0} & \mathbf{0} \end{pmatrix}(\mathbf{V}_1\mathbf{V}_2)^\mathbf{T} = \mathbf{U}_1\mathbf{S}_1\mathbf{V}_1^\mathrm{T} \tag{6}$$

where, $\mathbf{U}$ and $\mathbf{V}$ are unitary matrices with an appropriate size; $\mathbf{S}$ is a diagonal matrix with non-negative elements. Diagonal elements of $\mathbf{S}$ are known as singular values of $\boldsymbol{O}_i$. Singular values in $\mathbf{S}$ are listed in descending order. Therefore, the components in $\mathbf{U}_1\mathbf{S}_1\mathbf{V}_1^\mathbf{T}$ include most of the information defining the elements in $\boldsymbol{O}_i$. Components in $\mathbf{U}_2\mathbf{S}_2\mathbf{V}_2^\mathbf{T}$ are regarded as trivial components. The optimal state sequence predicted by the Kalman filter in a least squares sense is obtained as shown below.

$$\mathbf{X}_\mathrm{i} = \mathbf{S}_1^{1/2}\mathbf{V}_1^\mathrm{T} \tag{7}$$

where $\mathbf{X}_\mathrm{i} = [\mathbf{x}(i) \quad \mathbf{x}(i+1) \quad \dots \quad \mathbf{x}(i+j-1)]$.

The system matrices are obtainable from $\mathbf{X}_\mathrm{i}$. The number of poles corresponds to the number of singular values determined in Eq. (6). In other words, we can extract the modal response of the bridge from the measured acceleration data by the SVD.

2.2 System Identification based on Bayesian Approach during flood

The data consists of the measured acceleration time history denoted by $\ddot{\boldsymbol{x}}_j \in R^n$ $(j = 1, \dots, N)$, where n denotes measured degrees of freedom and N is the number of samples per measurement channel. Assuming classical damping, the data can be represented as shown in Eq. (8).

$$\ddot{\boldsymbol{x}}_j = \sum_{i=1}^{m} \boldsymbol{\phi}_i \, \ddot{\eta}_i(t_j) + \boldsymbol{\epsilon}_j \tag{8}$$

where the sum is over all contributing modes; $\boldsymbol{\epsilon}_j$ is the prediction error; $\boldsymbol{\phi}_i \in R^n$ is the mode shape confined to the measured dofs; $\eta_i(t)$ is the ith modal response satisfying the uncoupled modal equation shown in Eq. (9).

$$\ddot{\eta}_i(t) + 2\zeta_i\omega_i\dot{\eta}_i(t) + \omega_i^2\eta_i(t) = p_i(t) \tag{9}$$

where ω_i, ζ_i, p_i are the natural angular frequency, damping ratio and modal force, respectively. θ consists of the natural frequency, damping ratio and mode shape of the modes of interest. Other parameters are to be discussed later.

A Bayesian formulation based on the Fast Fourier Transform is first reported by Yuen and Katafygiotis (2003). Fast algorithms that allow practical implementation have been recently developed by Au (2011). Specifically, the data is represented in terms of its FFT, i.e., $D = \{F_k\}$, where

$$F_k = \sqrt{\frac{2\Delta t}{N}} \sum_{j=1}^{N} \ddot{\boldsymbol{x}}_j \exp\left[-\frac{2\pi\mathbf{i}(k-1)(j-1)}{N}\right] \tag{10}$$

with Δt is the sampling interval. For $k = 2,3, \dots N_q$, the FFT corresponds to frequency $\mathrm{f}_k = (k - 1)/N\Delta t$, where $N_q (= N/2 + 1)$ is the frequency index at the Nyquist frequency. If the FFTs in the full bandwidth are used, the representations in terms of time-domain data or frequency-domain data are equivalent because they are related by an invertible transformation.

In the frequency-domain approach, determining the likelihood function requires deriving the probability distribution of the FFT data for given θ. Elegant results can be obtained for sufficiently high sampling rate and long data duration often encountered in practice. In this case, as a standard result in spectral analysis (Schoukens and Pintelon 1991), the FFTs at different frequencies are asymptotically independent. The real and imaginary part of F_k are jointly Gaussian with zero mean and a covariance matrix is given by

$$\mathbf{C}_k = \frac{1}{2}\begin{bmatrix} \boldsymbol{\Phi}\mathrm{Re}\,\mathbf{H}_k\boldsymbol{\Phi}^{\mathrm{T}} & -\boldsymbol{\Phi}\mathrm{Im}\,\mathbf{H}_k\boldsymbol{\Phi}^{\mathrm{T}} \\ \boldsymbol{\Phi}\mathrm{Im}\,\mathbf{H}_k\boldsymbol{\Phi}^{\mathrm{T}} & \boldsymbol{\Phi}\mathrm{Re}\,\mathbf{H}_k\boldsymbol{\Phi}^{\mathrm{T}} \end{bmatrix} + \frac{S_e}{2}\mathbf{I}_{2n} \tag{11}$$

where $\boldsymbol{\Phi} = [\boldsymbol{\phi}_1, \boldsymbol{\phi}_2, \dots, \boldsymbol{\phi}_m] \in R^{n\times m}$; S_e is the spectral density of the prediction error; $\mathbf{I}_{2n}$ denotes the 2n×2n identity matrix; and Im and Re denote the real and imaginary parts, respectively; $\mathbf{H}_k \in C^{m\times m}$ is the theoretical spectral density matrix of the modal acceleration responses and is given by Eq. (12).

$$\mathbf{H}_k = \mathrm{diag}(\boldsymbol{h}_{\mathrm{k}})\,\mathbf{S}\,\mathrm{diag}(\boldsymbol{h}_k^*) \tag{12}$$

Here $\mathbf{S} \in C^{m\times m}$ is the spectral density matrix of modal forces; diag(·) denotes a diagonal matrix with the ith diagonal element equal to h_{ik}; an asterisk denotes a conjugate transpose; $\boldsymbol{h}_{\mathrm{k}} \in C^m$ is a vector of modal transfer functions with the element equal to

$$h_{ik} = [(\beta_{ik}^2 - 1) + \mathbf{i}(2\zeta_i\beta_{ik})]^{-1} \tag{13}$$

where, $\beta_{ik} = f_i/\mathrm{f}_k$ is a frequency ratio.

Using the above result for the likelihood function and adopting a uniform prior distribution, the resulting posterior PDF is given by Eq. (14).

$$p(\theta|\{D,M\}) \propto \exp[-L(\theta)] \quad (14)$$

where $L(\theta)$ is the NLLF (negative log-likelihood function) given by Eq. (15).

$$L(\theta) = \frac{1}{2}\sum_k \ln|\mathbf{C}_k(\theta)| + \frac{1}{2}\sum_k \boldsymbol{Z}_k^T \mathbf{C}_k(\theta)^{-1} \mathbf{Z}_k \quad (15)$$

where, $\boldsymbol{Z}_k$ contains the real and imaginary part of F_k. The sums in Eq. (15) indicate summation of all frequencies in the selected frequency band only. Here, the set of modal parameters θ consists of the natural frequencies f_i, damping ratios ζ_i, mode shape matrix $\boldsymbol{\phi}_i$, PSD matrix $\mathbf{S}$ of modal forces and PSD S_e of the prediction error for the modes of interest in the selected band.

3 TARGET BRIDGE AND MONITORING INFORMATION

The target bridge is a single railway track steel plate girder bridge. Height of the target pier is 11m and width is 2.5m. As there is high potential risk of scouring on the target pier, the long-term scour monitoring has been being carried out. The photo of the target bridge pier is shown in Figure 1. The elevation and plan views of the target bridge are shown in Figure 2. Eight triaxial sensors were installed on the top of the pier and connecting girders for the impact test as shown in Figure 2 a). All sensors except two sensors installed upstream and downstream of the pier top were removed after the impact test. Two sensors left on the pier top (see Figure 2b) are for the long-term ambient vibration monitoring. The sampling frequency of the measurement was 200Hz. A laser water level meter is installed on the target bridge.

Figure 1. Photo of target bridge pier.

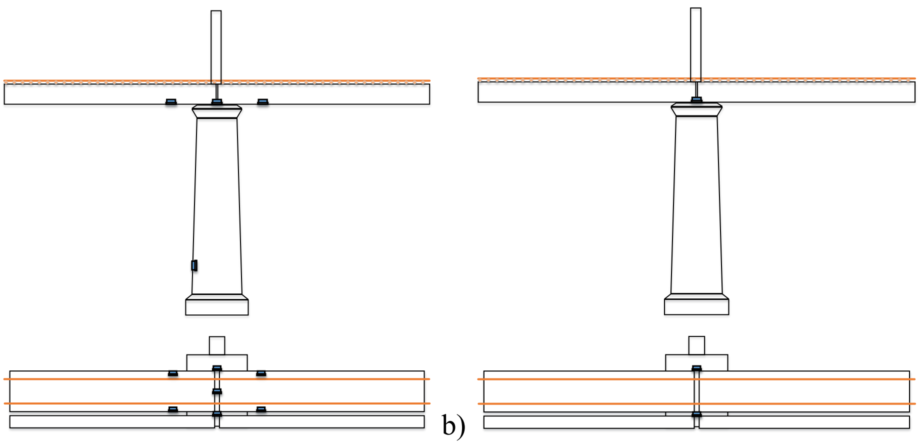

a) b)

Figure 2. Elevation view and plan view of the acceleration sensor installation position: a) for the impact test b) for the long-term ambient vibration monitoring.

4 MODE IDENTIFICATION OF TARGET BRIDGE

Modal characteristics of the bridge pier were identified from the vibration data excited during the impact test. Stability criteria that extracts stable vibration modes (Chang and Kim, 2016) are used to identify the modal properties of the bridge. Figure 3 shows the stabilization diagram (SD) in which the horizontal and vertical axes respectively stand for the frequency and model order. The black dots show the modal frequencies estimated from each of the model orders. The red circles indicate stably estimated modes that satisfy predefined deviation tolerances of the modal properties, i.e. the natural frequencies, damping ratio, and mode shapes. This study adopted the frequency deviation tolerance of 0.25 Hz, the damping deviation tolerance of 0.1 %, and the lower bound of Modal Assurance Criteria (MAC) of 0.95.

The vertical blue broken lines show dominant modes that appear stably throughout a wide range of model order and satisfy the deviation tolerances. The dominant frequency was identified at 9.2Hz. Figure 4 shows the mode shape of the dominant mode. As shown in Figure 4, this mode shape is relevant to the transversal rocking mode of the pier.

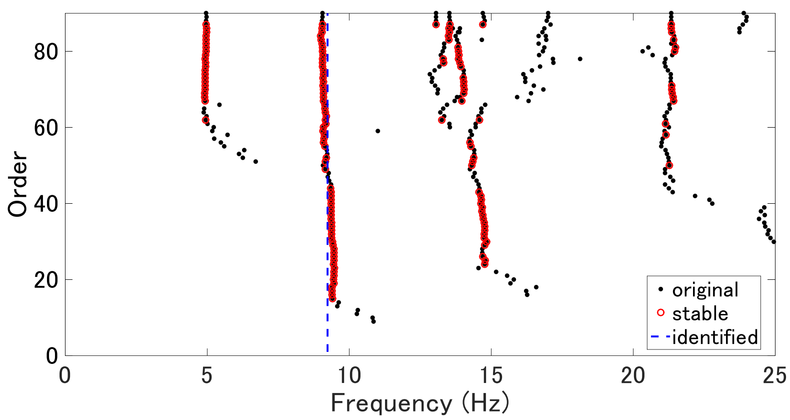

Figure 3. Stabilization Diagram (SD).

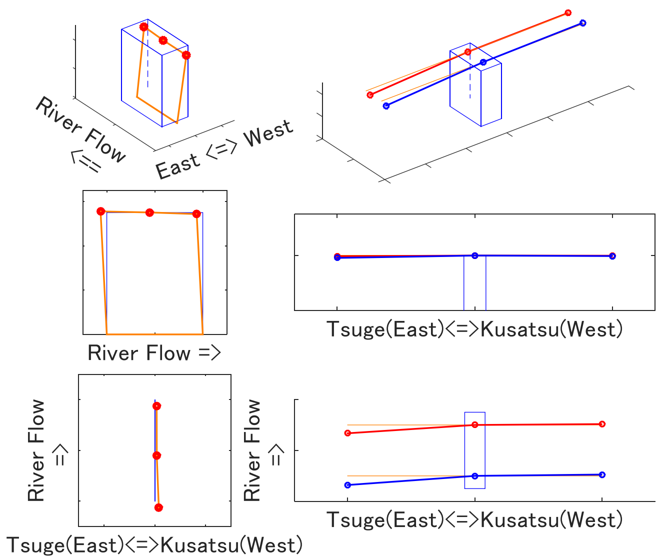

Figure 4. Identified mode shape (9Hz).

5 DOMINANT FREQEUNCY OF TARGET PIER DURING FLOOD

On September 20 in 2018, typhoon no.24 was approached and daily precipitation was 114mm, and ambient vibrations monitored on September 30 and October 1 were investigated to the identify dominant frequency of the target pier during flood.

The results are shown in Figure 5 and 6. Here, the frequency is estimated every minute. Horizontal axis stands for time, and the vertical axis stands for identified frequencies, wind speed, and water level respectively. It should be noted that "water level" represents the distance between water surface and lower flange of the bridge girder: e.g. the higher water surface goes up, the smaller the measured water level is. During 0:00 to 20:00 on September 30, before flood, identified frequencies were scattered. However, during a flood condition, i.e. 20:00 on September 30 to 6:00 on October 1, the frequency was stably identified. Histograms of the identified frequency are separately given with respect to the water level in Figure 7. Assuming all of the distributions follow normal distribution, the mean and variance are estimated as also summarized in Figure 7. The identified frequency decreases as the water level rises, the variance of the identified frequency also decreases. The influence of the additional mass due to flood might be a reason for the decrease of the frequency during flood (Samizo 2014). It shows that the natural frequency of the bridge pier is identified with high accuracy during the flood condition.

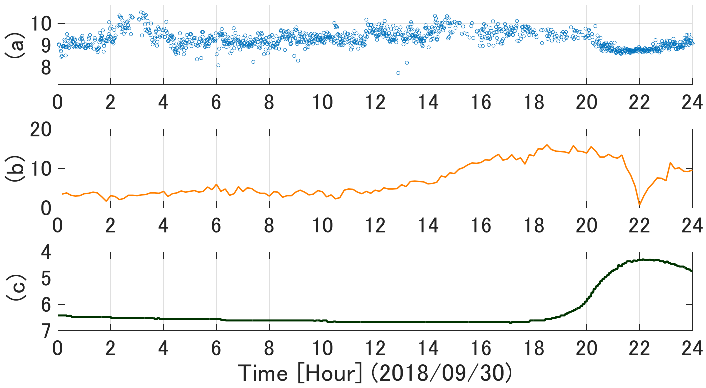

Figure 5. Monitoring data on September 30, 2018: (a) Frequency [Hz]; (b) wind speed [m/s]; (c) water level [m].

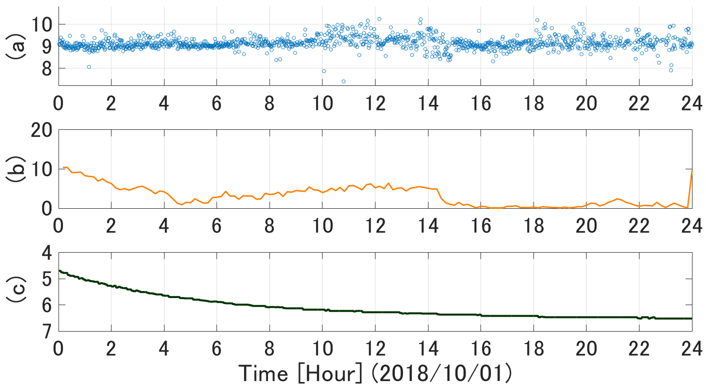

Figure 6. Monitoring data on October 1, 2018: (a) Frequency [Hz]; (b) wind speed [m/s]; (c) water level [m].

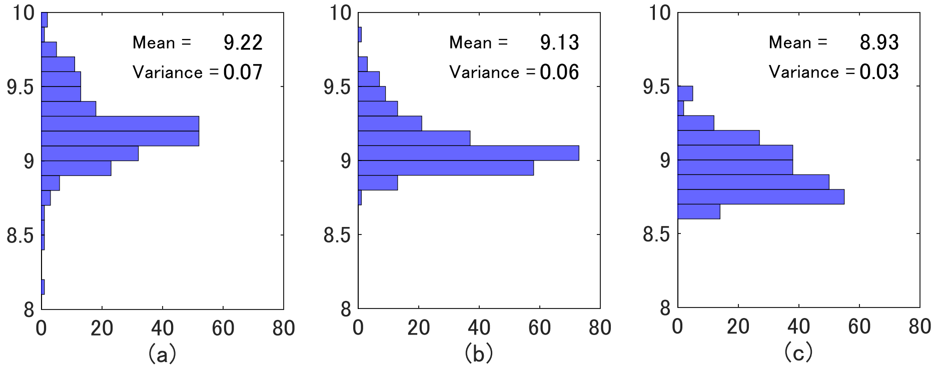

Figure 7. Identified frequency distribution: (a) water level more than 6m; (b) water level between 5m and 6m; (c) water level between 4m and 5m.

Figure 8 shows that the histogram of identified frequencies under the water level between 4m and 5m, i.e. during flood. Assuming that the distribution is a normal distribution, the blue broken line is set so that the probability of exceeding the blue line is about 2%. The blue solid line is the approximate curve of the distribution of the identified frequency. Occurrence of scour during flood is examined following the guideline of Japanese government (Ministry of Land, Infrastructure, Transport and Tourism 2007). In the guideline, occurrence of scour is decided if it is observed that 85% or less than the natural frequency in the health condition. Therefore, the frequency of 85% of the natural frequency in the health condition is adopted as a threshold of occurrence of scouring. The vertical red solid line in Figure 7 shows 85% of the natural frequency in the healthy condition (7.84 Hz). The probability of exceeding this red line is lower than 0.001%, which indicates extremely low possibility of scour occurrence during this flood.

Figure 9 shows that distribution of the identified frequencies before and after the flood. Mean values of the identified frequencies are 9.23Hz and 9.19Hz, which also indicates low possibility of scour occurrence.

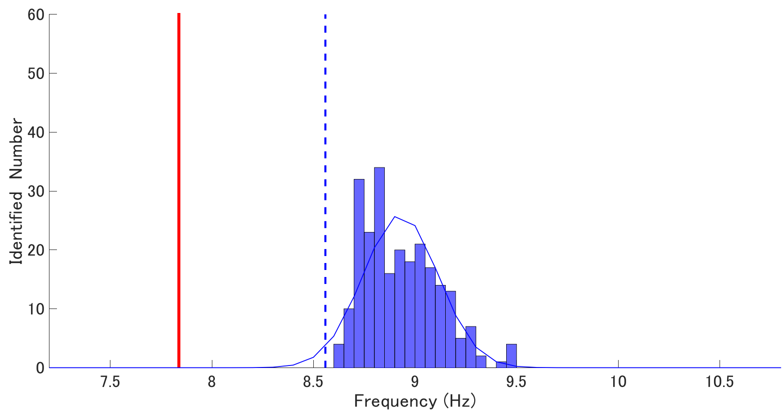

Figure 8. Histogram of identification frequencies from ambient vibrations (water level between 4m and 5m).

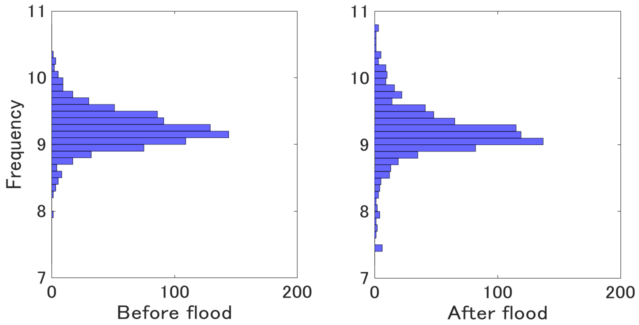

Figure 9. Distribution of natural frequency before and after the flood.

6 CONCLUSION

This study investigates a way of scour detection by means of ambient vibration monitoring of the bridge pier during flood. The natural frequency of the bridge pier was identified with high accuracy from the ambient vibration during the flood condition. The probability of exceeding the threshold for the scour was lower than 0.001%. Observations demonstrated extremely low possibility of scour occurrence during this flood.

REFERENCES

Keyaki, T. and Suzuki, O., 2013, Development of a new scour detector that enables monitoring of pier soundness, JR EAST Technical Review-No.27 Special edition paper. (in Japanese)

Heylen, W., Lammens, S. and Sas, P., 1997, Modal analysis theory and testing, K.U. Leuven, Belgium.

van Overschee, P. and De Moor, B., 1996, Subspace identification for linear systems, Kluwer Academic Publishers.

Goi, Y. and Kim, C.W., 2016, Mode identifiability of a multi-span cable-stayed bridge utilizing stabilization diagram and singular values, Smart Structures and Systems, 17(3), 391 - 411.

Au, S.K., 2011, Fast Bayesian FFT method for ambient modal identification with separated modes, J Eng Mech ASCE, 137(3), 214-226

Au, S.K., Zhang, F.L. and Ni, Y.C., 2013, Bayesian operational modal analysis: theory, computation, practice, Computers & Structures, 126, 3-14.

Goi, Y., Kim, C.W. and Au., S.K., 2016, Investigation of operational modal identification of a cable-stayed bridge based on Bayesian estimation considering stochastic uncertainty, J. of JSCE A2, 72(2): I_751-I_762. (in Japanese)

Yuen, K.V. and Katafygiotis, L.S., 2003, Bayesian Fast Fourier Transform approach for modal updating using ambient data, Adv Struct Eng., 6(2), 81-95.

Schoukens, J. and Pintelon, R., 1991, Identification of linear systems' a practical guideline for accurate modeling, London: Pergamon Press.

van Overschee and De Moor, 1993, Subspace algorithms for the stochastic identification problem, Automatica, 29(3), 649-660.

Chang, K.C. and Kim, C.W. 2016, Modal-parameter identification and vibration-based damage detection of a damaged steel truss bridge, Engineering Structures, 122, 156-173.

Samizo, M, 2014, A study on the evaluation of stability of railway bridge piers during the swelling of a river, 126-135.

Ministry of Land, Infrastructure, Transport and Tourism, Railway Bureau, 2007, Railway structures maintenance management standard and commentary (structural edition), 169-170.